

# **1 Non-parabolicity and band gap re-normalisation in Si doped ZnO**

2 R. E. Treharne\* and L. J. Phillips, K. Durose

3 *Stephenson Institute for Renewable Energy, University of Liverpool, UK*

4 (Dated: May 28, 2013)

## **Abstract**

5 PACS numbers: 78.20.Jq, 88.66.sq, 81.15.-z

6 Keywords: zinc oxide; magnetron sputtering; thin-film; doping; non-parabolicity, band gap normalisation

## 7 INTRODUCTION

## 8 EXPERIMENTAL METHODS

Films were deposited via RF magnetron sputtering using an AJA Phase II-J Orion system. The system was configured with a 'sputter-up' geometry with the substrate being suspended above two separate ceramic targets of ZnO and SiO<sub>2</sub> that were arranged off-centre and tilted at 5° towards the middle of the substrate. Soda-lime glass substrates (OptiWhite<sup>TM</sup>, NSG) of size 100 × 100 × 4 mm<sup>3</sup> were used throughout. They were cleaned by scrubbing with a nylon brush and a series of de-ionized water and isopropanol alcohol rinses followed by blow drying with a nitrogen gas jet. During deposition the ZnO and SiO<sub>2</sub> targets were sputtered from simultaneously using powers of 150 W and 50 W respectively. A growth pressure of 2mTorr Ar was used during deposition. The substrate temperature was maintained at 350 ± 5°C during growth and the substrate was kept static (i.e was not rotated). Deliberate gradients of both thickness and composition were subsequently achieved across the resultant film to generate a 'combinatorial' sample. A second film of pure SiO<sub>2</sub> was deposited under identical conditions (but without ZnO) to generate a reference film for calculating the % wt. profile of SiO<sub>2</sub> in the co-sputtered film.

A Shimadzu UV-Vis-IR 3700 spectrophotometer with mapping capability was used to measure the transmittance of the co-sputtered film over the range 250 - 2500 nm. 289 spectra were taken in total at 5 mm increments over the full sample surface. At each of these 289 points the sheet resistance was also measured using a CMT-SR2000 4-point probe mapping system. Following transmittance and sheet resistance measurements the sample was cut into one hundred 10 × 10 mm<sup>2</sup> pieces. A selection of these pieces, 10 in total, were further scribed into four 5 × 5 mm<sup>2</sup> sections and Hall measurement were performed on each of these sections. The Hall measurement was performed with custom built equipment, provided by Semimetrics Ltd., using a field strength of 0.8 T. Ellipsometry was performed on the same sections using a Woollam M2000-UI system. Ellipsometry was also used to map the thickness profile of the pure SiO<sub>2</sub> reference film.

## 34 RESULTS

### 35 Fitting of optical spectra

36 Figure 1 shows a typical transmittance spectra taken from a single point on the combina-  
37 torial ZnO:Si sample. The full details of the model of the dielectric permittivity,  $\varepsilon(\omega)$ , used  
38 to fit the data are given in [1]. The key components of the model include: 1) a Lorentzian  
39 oscillator to account for the behaviour of the system's bound electrons and to provide a  
40 smoothly varying dielectric background over the range of interest (250 – 2500 nm), 2) an  
41 extended Drude model [2], to characterise the system's free electron response, and 3) an  
42 inter-band transition model to account for the steep increase in the material's absorption  
43 coefficient ( $\alpha \propto (E - E_G)^{1/2}$ ) in the vicinity of its direct band gap (3.3 – 3.4 eV). The two  
44 key parameters extractable from the dielectric model are the film's thickness,  $d$ , and plasma  
45 frequency,  $\omega_p$ , which is related directly to the carrier concentration according to

$$\omega_p = \sqrt{\frac{n_e e^2}{m_e \varepsilon_0}} \quad (1)$$

46 where  $m_e$  is the effective electrons (expressed in units of the free electron mass,  $m_0$ ) and  $\varepsilon_0$   
47 is the permittivity of free space.

48 Fitting was achieved by using a Nelder-Mead downhill simplex algorithm [3], implemented  
49 via python script, to minimize the quantity

$$\chi^2 = \sum_i^N \sqrt{\frac{y_i - O_i}{N^2}} \quad (2)$$

50 where  $N$  is the total number of data points in the spectra,  $O_i$  the observed transmittance at  
51 each wavelength over the range of interest, and  $y_i$  the theoretical transmittance calculated  
52 using the transfer matrix method [4] for a single thin-film on a finite, transparent substrate.  
53 The fitting algorithm was iterated until the relative fractional change in consecutive  $\chi^2$   
54 values was less than  $1 \times 10^{-6}$ . The fitting of all 289 transmittance spectra taken over the  
55 combinatorial sample was fully automated, the only user input required being an initial  
56 estimate of film thickness at the point of the first spectrum. This automation ensured that  
57 the fitting of consecutive spectra was highly consistent. For all spectra,  $\chi^2$  values of  $< 1$   
58 were achieved indicating that all fits were as successful as that shown in figure 1.

59 It was not possible to extract accurate values for the optical band-gap  $E_G$  from the inter-  
60 band transition component of the model. All values were typically  $\sim 0.2$  eV lower than

61 expected (even once non-parabolicity and re-normalisation effects had been accounted for,  
 62 see sections and ). This is due to the presence of a population of impurity states located in  
 63 energy just below the bottom of the conduction band. The presence of these states generate  
 64 a broadening, commonly referred to as an ‘Urbach tail’ [5], in the onset of the absorption  
 65 coefficient. It is very difficult to determine the extent of this broadening by fitting the  
 66 dielectric model to a single transmittance spectra. The use of variable angle spectroscopic  
 67 ellipsometry (VASE) was therefore necessary to determine the true band gap of the material.  
 68 For each point over the combinatorial sample surface a set of three ellipsometric spectra,  
 69 taken at angles of 60, 65 and 70° with respect to a plane normal to the sample surface, was  
 70 measured and fitted using a parameterized semi-conductor (PSEMI-M0) model [6] over the  
 71 range 350 – 1000 nm. The use of multiple spectra allowed the effect of the tail states to be  
 72 extricated from the direct band to band transitions. Figure 2 shows the difference in the  $\alpha^2$   
 73 versus  $E$  behaviour extracted from transmittance and ellipsometry data respectively. This  
 74 disparity between band gaps extracted from the two techniques has been reported previously  
 75 by Srikant [7].

## 76 **Conduction band non-parabolicity**

77 For highly doped metal-oxides it has been shown that the conduction band,  $E_c$ , is ‘non-  
 78 parabolic’ and that the origin of this non-parabolicity may be attributed to a carrier de-  
 79 pendent effective mass,  $m_e(n_e)$ . The functional form of this dependence, first suggested by  
 80 Pisarkiewicz *et. al* [8], is given by

$$m_e(n_e) = m_{e0} \sqrt{1 + \frac{2C\hbar^2 k}{m_{e0}}} \quad (3)$$

81 where  $m_{e0}$  is the value of the effective mass at the conduction band minimum and  $C$  is the  
 82 non-parabolicity factor, expressed in  $\text{eV}^{-1}$ . The carrier wave-number can be expressed in  
 83 terms of the carrier concentration according to  $k = (3\pi^2 n_e)^{1/3}$ . By re-examining equation  
 84 1 it is clear that the relationship between  $\omega_p^2$  and  $n_e$  is becomes non-linear if the effective  
 85 mass is not a constant. Figure 3 shows a plot of  $\omega_p$ , extracted from the spectrophotometry  
 86 measurements, versus the carrier concentration,  $n_e^H$ , determined via Hall measurements, for  
 87 the sample subset cut from the original combinatorial sample. A similar  $\chi^2$  minimization  
 88 procedure to that described in section , in which the fitting parameters were  $m_{e0}$  and  $C$ ,

89 was applied to the data set using

$$\chi^2 = \sum_{i=1}^n \frac{(n_{ei}^S - n_{ei}^H)^2}{n^2} \quad (4)$$

90 where the superscript  $S$  corresponds to carrier concentrations calculated, using a carrier  
 91 dependent effective mass  $m_e(n_e)$  (equations (1) a 3), from the spectroscopically determined  
 92 plasma frequencies. The superscript  $H$  denotes values of  $n_e$  determined directly via Hall  
 93 measurements. To determine the uncertainty associated with the fitted  $m_{e0}$  and  $C$  values a  
 94 Monte-Carlo style error treatment [9] was implemented within which the  $\chi^2$  minimization  
 95 procedure was performed 1000 times. The inset plot in figure 3 shows the mean  $m_e(n_e)$   
 96 relationship (solid line) and the corresponding spread (yellow line). An average extracted  
 97 value of  $m_{e0} = 0.35 \pm 0.02m_0$  is higher than previous published values of  $0.24 - 0.28m_0$  for  
 98 the effective mass in undoped ZnO. An average extracted value of  $C = 0.30 \pm 0.01$  eV agrees  
 99 very well with previously reported values of  $\sim 0.29$  eV<sup>-1</sup> [10, 11] for Al doped ZnO films.

## 100 **Band-gap renormalization**

101 The optical band gap of a degenerately doped metal-oxide system increases as a function  
 102 of carrier concentration (Burstein-Moss shift [12, 13] according to

$$E_G = E_{G0} + \frac{\hbar^2(3\pi^2n_e)^{2/3}}{2m_{eff}} \quad (5)$$

103 where  $E_{G0}$  is the band-gap at the conduction band minimum and the joint density of states  
 104 effective mass,  $m_{eff}$  is given as

$$\frac{1}{m_{eff}} = \frac{1}{m_h} + \frac{1}{m_e(n_e)} \quad (6)$$

105 A constant hole effective mass value of  $m_h = 0.7m_0$  [] is assumed throughout this work. Note  
 106 that the non-parabolicity of the conduction band is accounted for when estimating the band  
 107 gap by using the carrier dependent effective mass  $m_e(n_e)$  determined in section . The data  
 108 points in figure 4 show the band-gap values, determined via ellipsometry, plotted against the  
 109 Hall carrier concentrations. The points lie some distance from the relationship predicted by  
 110 equation 5. The apparent reduction in the real band-gap values is due the re-normalization  
 111 effects of many body electron-electron, electron-ion and hole-hole interactions. Lu *et. al*

112 [14] have shown that the total energy shift due to re-normalization can be estimated by  
 113 parameterising the detailed model described by *Jain et. al* according to

$$E_R = An_e^{1/3} + Bn_e^{1/4} + Cn_e^{1/2} \quad (7)$$

114 where  $E_R$  is negative with respect to  $E_G$ . The  $n_e^{1/3}$ ,  $n_e^{1/4}$  and  $n_e^{1/2}$  dependencies correspond to  
 115 the exchange energy of free electrons, their correlation energy and the electron-ion interaction  
 116 energy respectively. The coefficients  $A$ ,  $B$ , and  $C$ , quantify the strength of each of these three  
 117 dependencies. The coefficient values for the data shown in figure 4, and a value for  $E_{G0}$ , was  
 118 extracted using the established minimisation procedure. Table I show the extracted values  
 119 and comparative values for n-type ZnO thin-films. The strength of the  $n_e^{1/3}$  dependence is  
 120 roughly three times than that reported for Al doped ZnO.

## 121 MAPPING OF COMPOSITIONAL DEPENDENCE

122 Film thickness profiles were determined for the combinatorial ZnO:Si and SiO<sub>2</sub> samples.  
 123 The % wt. SiO<sub>2</sub> content at each point over the combinatorial sample was estimated according  
 124 to

$$x = \frac{\Gamma_B d_B}{\Gamma_A d_A + \Gamma_B d_B} \times 100\% \quad (8)$$

125 where  $\Gamma_A$  and  $\Gamma_B$  are the bulk densities of ZnO and SiO<sub>2</sub> respectively and  $d_A$  and  $d_B$  are the  
 126 corresponding thicknesses,  $d$ , of the ZnO and SiO<sub>2</sub> films. The carrier concentration profile  
 127 for the combinatorial sample was calculated from extracted  $\omega_p^S$  values according to equation  
 128 1 and using the non-parabolic effective mass relationship,  $m_e(n_e)$ , determined in section .  
 129 The corresponding mobility profile was calculated according to

$$\mu_e = \frac{1}{n_e^S R_S d e} \quad (9)$$

130 where  $R_S$  are the sheet resistance values obtained directly from 4 point probe measurements.  
 131 Figure 3 shows the three dimensional contour profiles of  $n_e$  and  $\mu_e$  accross the surface of  
 132 the combinatorial sample. In both cases, a maximal ridge, corresponding to  $n_e \sim 4.5 \text{ cm}^{-3}$   
 133 an  $\mu_e \sim 16 \text{ cm}^2 \text{V}^{-1} \text{s}^{-1}$ , runs diagonally across the sample. By superimposing the contour  
 134 distribution of % wt. SiO<sub>2</sub> content (dotted black contour lines) a very strong correlation  
 135 between carrier concentration and composition becomes apparent, the maximum  $n_e$  and  $\mu_e$   
 136 values corresponding to a value of  $x = 0.65\%$  wt. SiO<sub>2</sub> content.

By plotting the distributions of  $n_e$  and  $\mu_e$  with respect to  $x$  the compositional dependence can be observed directly, see figure 4. Here the strength of the combinatorial analysis is fully appreciated by its ability to generate continuous, non-ambiguous distributions of the material's electrical behaviour and shows that it is highly sensitive to the composition - the resistivity spanning over three orders of magnitude within the compositional range  $x = 0 - 0.65\%$  wt.  $\text{SiO}_2$ . Furthermore, the uncertainty in the optimum value of  $x$ , that minimises the resistivity, is significantly reduced when compared to the multi-sample analyses that are commonly reported.

The solid straight line in the  $n_e$  vs  $x$  plot indicates the relationship predicted for 100% doping efficiency, i.e. where every Si atom incorporated into film substitutionally replace a Zn atom and contributes two free electrons to the system. For low values of  $x$ , i.e. in the range  $0 - 0.5\%$  wt.  $\text{SiO}_2$ , this relationship is adhered to. However as  $x$  increases further the doping efficiency decreases rapidly and the carrier concentration is limited to  $3 - 4 \times 10 \text{ cm}^{-3}$  for compositions up to  $10\%$  wt.  $\text{SiO}_2$ . After the optimum value of  $x$  is reached the mobility drops off steeply and approaches a value of zero for values of  $x$  beyond  $6\%$ . This suggests that as  $x$  is increased beyond the optimum composition, Si is no longer incorporated into the film as a substitutional dopant and substitutionally acts to increase the scattering of the free carriers existing as an interstitial impurities or forming segregated Si-O phases at the grain boundaries of the material.

## CONCLUSIONS

---

\* Corresponding Author: R.Treharne@liverpool.ac.uk

- [1] R. E. Treharne, K. Hutchings, D. A. Lamb, S. J. C. Irvine, D. Lane, and K. Durose, J. Phys. D: Appl. Phys **45**, 335102 (2012).
- [2] D. Mergel and Z. Qiao, J. Phys. D: Appl. Phys **35**, 794 (2002).
- [3] J. A. Nelder and R. Mead, The Computer Journal **7**, 308 (1965).
- [4] H. A. Macleod, *Thin-Film Optical Filters* (Adam Hilger Ltd, 1986).
- [5] Urbach, .

- 164 [6] C. Herzinger, B. Johs, W. McGahan, J. Woollam, and W. Paulson, Journal of Applied Physics  
165 **83**, 3323 (1998).
- 166 [7] V. Srikant and D. R. Clarke, J. Appl. Phys. **83**, 5447 (1998).
- 167 [8] T. Pisarkiewicz and A. Kolodziej, Phys. Stat. Sol. B **158**, K5 (1990).
- 168 [9] R. J. Mendelsberg, *Photoluminescence of ZnO grown by eclipse pulsed laser deposition*, Ph.D.  
169 thesis, University of Canterbury, New Zealand (2009).
- 170 [10] F. Ruske, A. Pflug, V. Sittinger, B. Szyszka, D. Greiner, and B. Rech, Article in press - Thin  
171 Solid Films.
- 172 [11] K. Ellmer, Journal of Physics D: Applied Physics **34**, 3097 (2001).
- 173 [12] E. Burstein, Physical Review **93**, 632 (1954).
- 174 [13] T. S. Moss, Proceedings of the Physical Society. Section B **67**, 775 (1954).
- 175 [14] J. Lu, S. Fujita, T. Kawaharamura, H. Nishinaka, Y. Kamada, T. Ohshima, Z. Ye, Y. Zeng,  
176 Y. Zhang, L. Zhu, *et al.*, J. Appl. Phys. **101**, 083705 (2007).



FIG. 1.

FIG. 2.

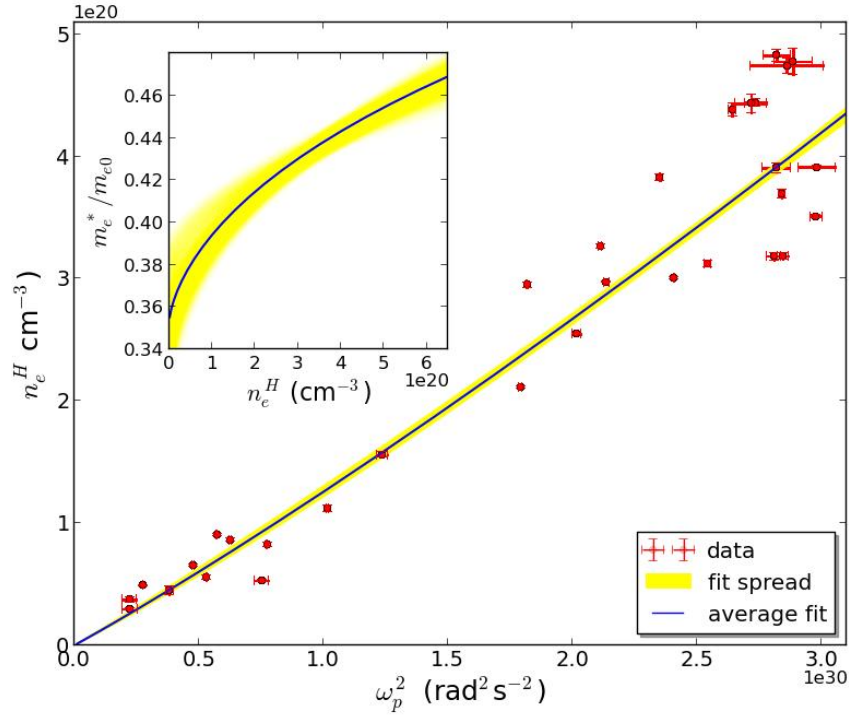


FIG. 3.

Parameter 1	Extracted Value	Copmparison [14]
$A (\times 10^{-8} \text{ eV.cm})$	$2.1 \pm 0.8$	0.69
$B (\times 10^{-7} \text{ eV.cm}^{3/2})$	$3.0 \pm 2.6$	1.6
$C (\times 10^{-7} \text{ eV.cm}^{3/4})$	$8.7 \pm 1.5$	7.76
$E_{G0} \text{ (eV)}$	$3.41 \pm 0.01$	-

TABLE I. This is the caption

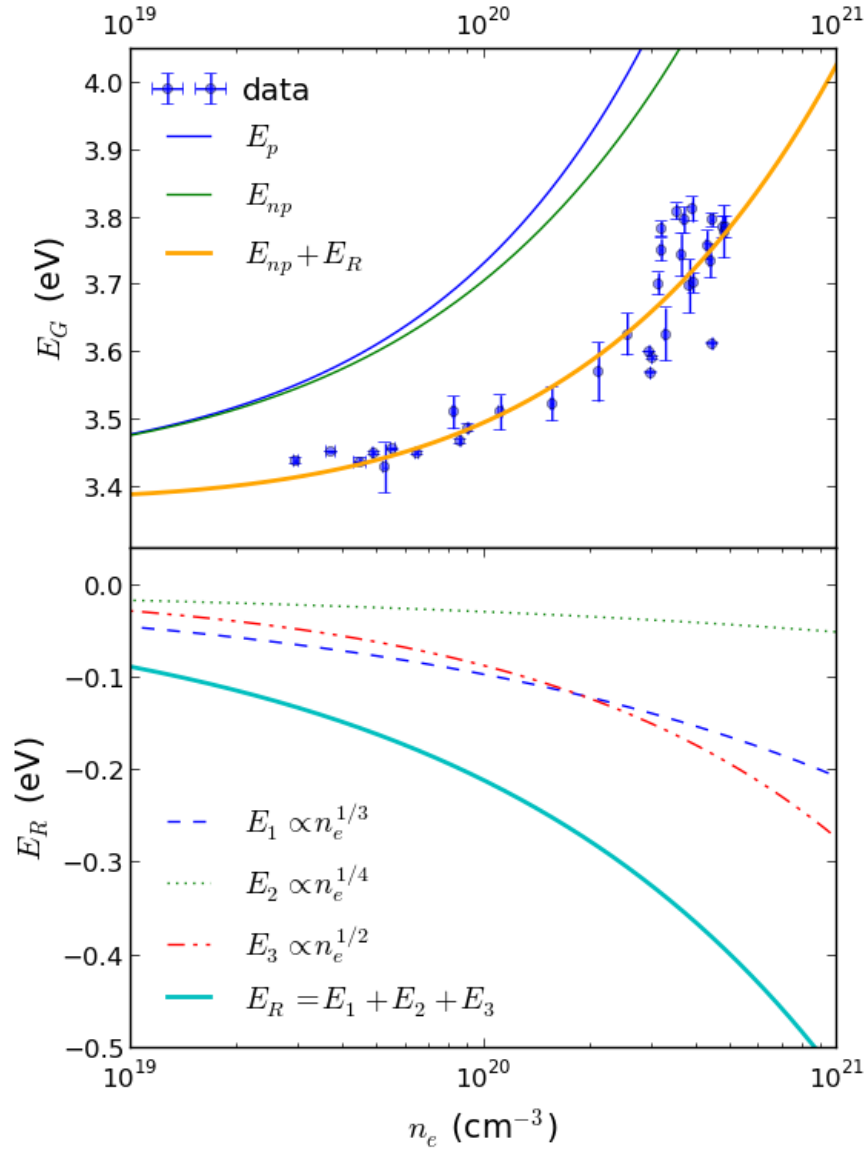


FIG. 4.

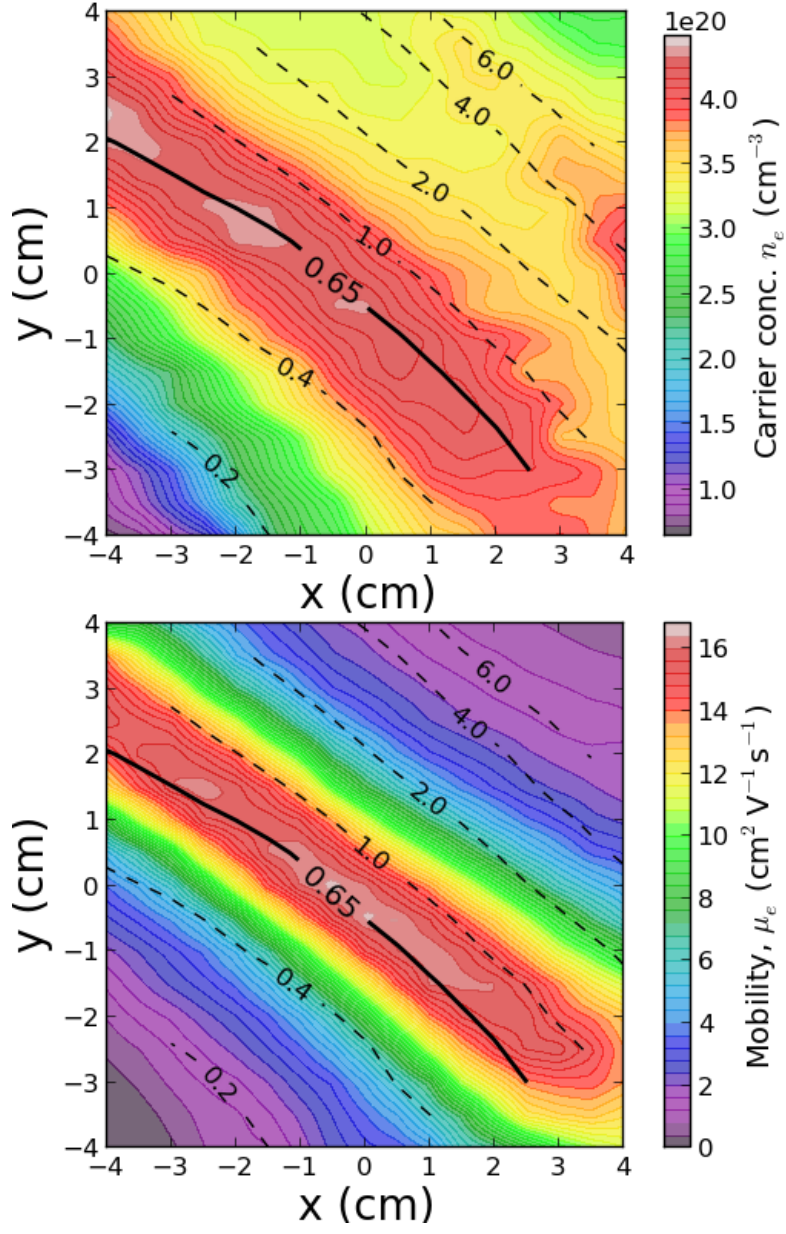


FIG. 5. Contour maps of carrier concentration and mobility over the combinatorial sample. The (—) contour lines show an overlay of the % wt.  $\text{SiO}_2$  composition.

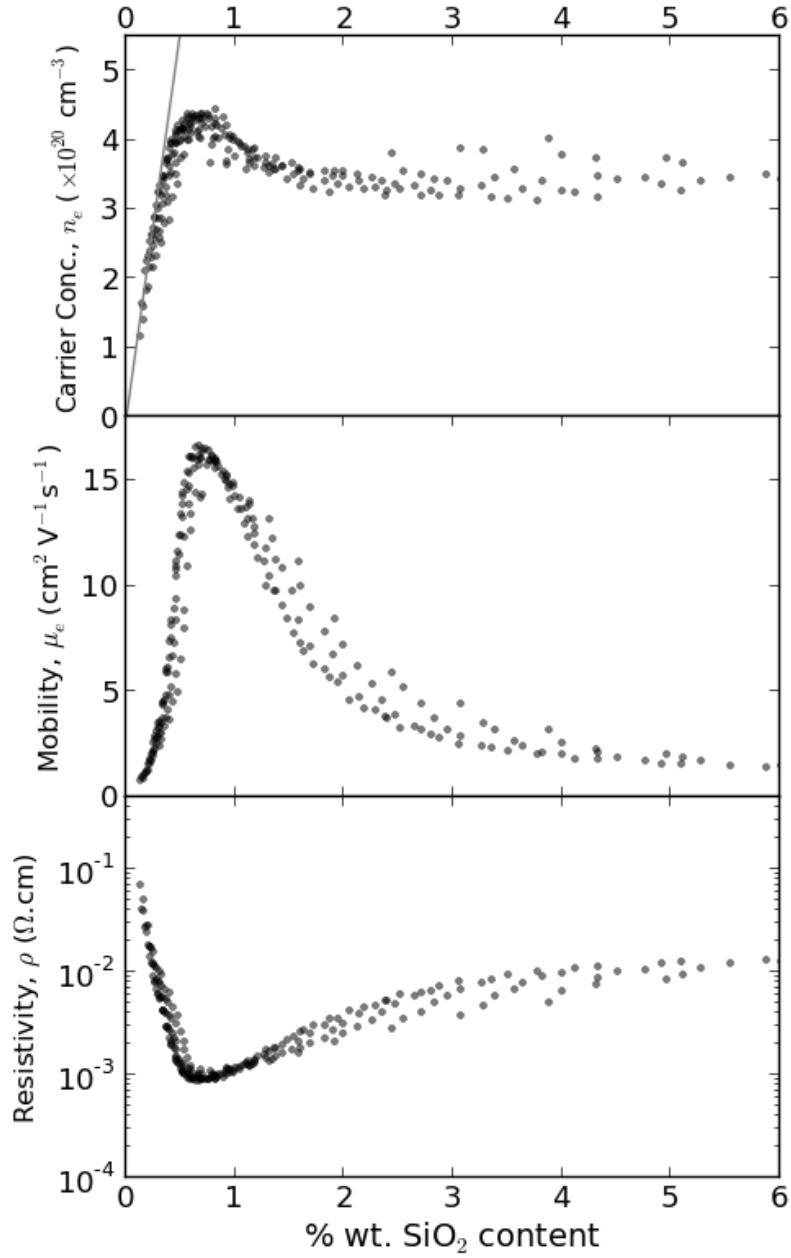


FIG. 6. Distributions of carrier concentration, mobility and resistivity with respect to % wt. SiO<sub>2</sub> content. The maximum values for  $n_e$  ( $4.4 \times 10^{20} \text{ cm}^{-3}$ ) and  $\mu_e$  ( $16.5 \text{ cm}^2 \text{ V}^{-1} \text{ s}^{-1}$ ) coincide with a composition of 0.65% wt. SiO<sub>2</sub>. The solid straight line in the top plot shows the maximum theoretical carrier concentration with respect to SiO<sub>2</sub> content should every incorporated Si atom be substituted at a Zinc site and donate 2 carriers.

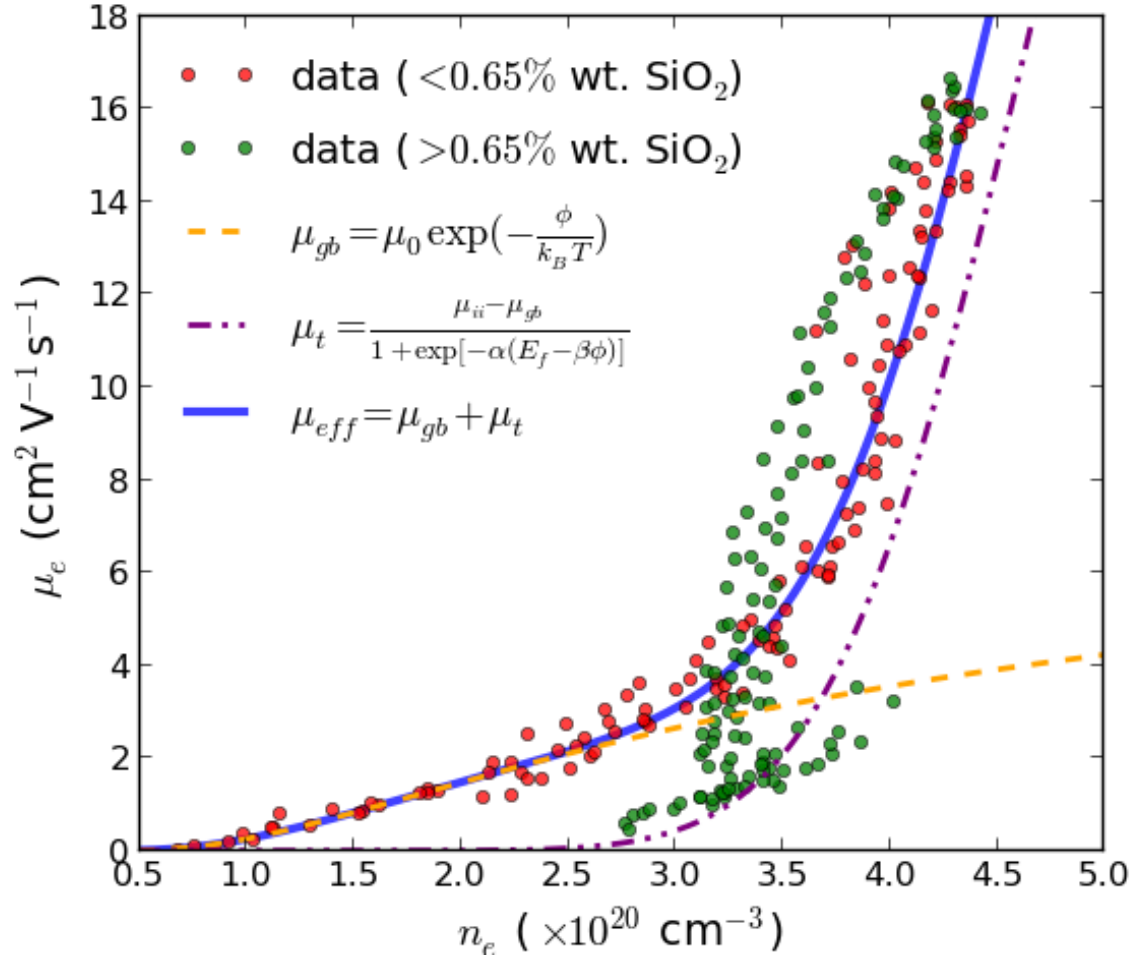


FIG. 7.